NASA Technical Memorandum 89133

DEVELOPMENT OF COMPUTATIONAL METHODS
FOR UNSTEADY AERODYNAMICS AT THE
NASA LANGLEY RESEARCH CENTER

E. Carson Yates, Jr.,
and Woodrow Whitlow, Jr.

MARCH 1987

NASA
National Aeronautics and
Space Administration

Langley Research Center
Hampton, Virginia 23665-5225

DEVELOPMENT OF COMPUTATIONAL METHODS FOR UNSTEADY AERODYNAMICS
AT THE
NASA LANGLEY RESEARCH CENTER

E. Carson Yates, Jr.
Chief Scientist
Loads and Aeroelasticity Division

Woodrow Whitlow, Jr.
Group Leader, Methods Development Group
Unsteady Aerodynamics Branch
Loads and Aeroelasticity Division
NASA Langley Research Center
Hampton, Virginia 23665-5225
U. S. A.

SUMMARY

The current scope, recent progress, and plans for research and development of computational methods for unsteady aerodynamics at the NASA Langley Research Center are reviewed. Both integral-equation and finite-difference methods for inviscid and viscous flows are discussed. Although the great bulk of the effort has focused on finite-difference solution of the transonic small-perturbation equation, the integral-equation program is given primary emphasis here because it is less well known.

INTRODUCTION

Progress in the development of computational methods for steady and unsteady aerodynamics has perennially paced advancements in aeroelastic analysis and design capabilities. These capabilities, in turn, are of growing importance in the analysis and design of high-performance aircraft as well as other types of flight vehicles. Consequently, considerable effort has been directed toward the development of appropriate unsteady-aerodynamic methodology in the NATO countries and elsewhere. This paper reviews the contributions to those efforts at the NASA Langley Research Center. Specifically, the current scope, recent progress, and plans for research and development of both integral-equation and finite-difference methods for inviscid and viscous flows are discussed, and example applications are shown. Although the great bulk of the effort in recent years has focused on finite-difference solution of the transonic small-perturbation equation, the integral-equation program is given primary emphasis here because it is less well known.

INTEGRAL-EQUATION METHODS

The Langley integral-equations program is directed toward general, accurate, efficient, and unified treatment of flows around vehicles having arbitrary shapes, motions, and deformations (including control motions) at subsonic, transonic, and supersonic speeds up to high angles of attack. Special attention is given to real-world design and operating conditions (e.g., Mach number, angle of attack, maneuver) as well as to efficient computation for both design and analysis applications. As will be brought out in the subsequent discussion, the integral-equation approach is well suited for these purposes because flow complexities such as viscous effects or transonic flow need to be addressed only in the flow regions where they actually occur, and there is no requirement for patching and matching flow domains or regional solutions. Moreover, for design applications repetitive and nonrepetitive portions of the computations are readily separable, and the required sensitivities of aerodynamic parameters to variations in aircraft geometry can be readily calculated. Although the integral-equations research program has been given only limited and intermittent support for the last several years, it has nevertheless produced some significant results.

Following a long-range plan established a number of years ago (fig. 1), initial efforts addressed the development of surface-panel methods for subsonic (refs. 1 to 5) and supersonic (refs. 1, 2, 6, 7) linearized potential flow. Current activities include nonlinear methods implementing the full-potential equation for high-subsonic/transonic/low-supersonic speeds (ref. 8). Although the initial high-subsonic/transonic proof-of-concept codes (refs. 9 to 11) implemented the small-perturbation potential equation, there is no particular benefit in refining codes for small-perturbation conditions or two-dimensional flow as stepping-stones toward more realistic conditions. Consequently, these items have been deleted from the original plan (fig. 1). Some computations for two-dimensional flow are made in order to conserve computer resources, however.

Another change from the original plan (fig. 1) shows that the Euler equations are not addressed explicitly in this program. Modification of the full-potential equation to account for entropy changes across shock waves (e.g., as in ref. 12) should greatly expand the usefulness of potential-flow solutions well into the range of flow conditions that would otherwise require Euler solutions. Consequently, for present purposes we go directly from the modified full-potential method to the Navier-Stokes equations which are being addressed by use of the classical Helmholtz scalar/vector-potential decomposition (refs. 13 to 15). Euler solutions may, of course, be obtained from Navier-Stokes methods with zero viscosity. We are specifically concerned with several types of viscous influences: Thin wakes separating from lifting-surface edges are well represented by inviscid-flow singularities (vortex sheets). Other viscous influences require solution of Navier-Stokes equations or equivalent. These influences include boundary-layer effects, especially on deflected and/or deflecting control surfaces, shock/boundary-layer interaction, and large areas of flow separation in general. Specifics of these problem areas are addressed in the subsequent sections of this paper.

The time-dependent full-potential partial differential equation

$$\nabla^2 \phi - \frac{1}{a_\infty^2} \left(\frac{\partial}{\partial t} + U_\infty \frac{\partial}{\partial x} \right)^2 \phi = F \tag{1}$$

is the governing equation for most of the work described herein. Application of the generalized Green's-function method to this equation yields an equivalent integral equation for the velocity potential ϕ at any point P in the flow or on the surface of a body in the flow at any time t (ref. 1).

$$\phi(P,t) = \underbrace{\int \int \int \int GF dV_1 dt_1}_{\text{nonlinear terms}}$$

$$+ \underbrace{\int \int \int \left[\nabla_1 S \cdot (G\nabla_1\phi - \phi\nabla_1 G) - \frac{1}{a_\infty^2} \frac{dS}{dt_1} \left(G \frac{\partial\phi}{\partial t_1} - \phi \frac{\partial G}{\partial t_1} \right) \right] |\square S|^{-1} dS dt_1}_{\text{linear terms}} \tag{2}$$

where ϕ is the perturbation velocity potential, G is the Green's function, F represents all the nonlinear terms, a_∞ is the freestream speed of sound, U_∞ is the freestream speed, x is the coordinate in the freestream direction, $S(x,y,z,t) = 0$ defines the body surface, and

$$|\square S| = \sqrt{S_x^2 + S_y^2 + S_z^2 + S_t^2}$$

The exact boundary condition on the body surface is

$$\frac{DS}{Dt} = 0 \tag{3}$$

The time integration with respect to t_1 in equation (2) is made trivial by choice of a subsonic or supersonic source pulse as the Green's function.

An important point here is that only the nonlinear terms need to be integrated over a fluid volume. The linear terms are integrated only over the surface of the body and its wake. Note also that the Green's function is a function of freestream Mach number, not local Mach number. Equations (2) and (3) have been formulated and computationally implemented in a moving frame of reference so that they are applicable to problems such as helicopter rotors and maneuvering aircraft as well as aircraft in uniform motion (refs. 16 to 19).

Linearized Theory

If perturbations from freestream velocity are small, and Mach number is not near one nor too high in the supersonic range, the non-linear terms are negligible, and the volume integral can be ignored. The remaining surface integral of the linear terms is discretized by surface paneling (ref. 2) (e.g., arbitrary twisted quadrilateral panels as in refs. 3 and 4). The unsteady-flow solution can then be obtained directly by integration in time domain, or a time solution by Laplace transform (refs. 2 to 4) converts to a complex-frequency domain formulation which is generally more efficient for use in solving linear aeroelastic problems.

The velocity potential on the paneled surface is then found in terms of the normalwash distribution which, in general, is known from the input shape, orientation, motion, and deformation.

$$[\bar{Y}_{jh}] \{\bar{\phi}_h\} = [\bar{Z}_{jh}] \{\bar{\Psi}_h\} \tag{4}$$

where $\bar{\phi}_h$ is the Laplace transform of the perturbation velocity potential, and $\bar{\Psi}_h$ is the Laplace transform of the normalwash

$$\bar{Y}_{jh} = \delta_{jh} - (C_{jh} + sD_{jh}) e^{-s\theta_{jh}} - \sum_h (F_{jn} + sG_{jn}) S_{nh} e^{-s(\theta_{jn} + \tau_n)} \tag{5}$$

$$\bar{Z}_{jh} = B_{jh} e^{-s\theta_{jh}} \tag{6}$$

2

δ_{jh} is Kronecker delta, s is the Laplace transform variable (complex frequency), $B_{jh}, C_{jh}, D_{jh}, F_{jn}, G_{jn}$ are integrals over surface panels, θ_{jh}, τ_{jn} are lag functions, and $S_{nh} = \pm 1$ for panels adjacent to a trailing edge on upper or lower surface of the body and is zero otherwise. Surface pressures are obtained from the potential by use of Bernoulli's equation.

Several features of equations (4) to (6) are significant. First, the elements of the Y and Z influence matrices are independent of the normalwash and hence independent of the mode of motion or deflection. Moreover, these matrix elements are simple functions of the complex frequency s so that the cost of changing frequency or calculating for multiple frequencies is small. The influence integrals B, C, and D represent integrals of source, doublet, and "ratelet" distributions over each body-surface panel, and integrals F and G are the corresponding doublet and "ratelet" integrals for wake panels. For a given paneling geometry, all of these integrals are functions only of Mach number. If a problem (e.g., dynamic response or flutter) involves multiple modes of normalwash, the normalwash vector in the equation becomes a matrix of modal columns, and the potential distributions for all the modes can be found in a single solution. Similarly, solutions for additional modes or revised modes (as in a structural-design optimization problem) can be obtained without recalculating the Y and Z matrices. For use in design processes, this formulation also appears to provide a general and very efficient means for evaluating sensitivities, i.e., changes in aerodynamic properties caused by changes in external shape. Demonstration calculations have been initiated.

The generality and versatility of this approach is indicated by its use by Rockwell International for flutter analysis of the space shuttle (fig.2) in the mid 1970's. Nearly 800 panels were used on the orbiter, and up to 60 modes of motion were used in both symmetric and antisymmetric flutter analyses. Subsequently, the external tank and solid rocket boosters were added, and the calculations were repeated for the entire launch configuration.

For development purposes equations (4) to (6) have been implemented in a prototype code called SOUSSA P1.1 (Steady, Oscillatory, and Unsteady Subsonic and Supersonic Aerodynamics - Version 1.1) (refs. 3 and 4) which is applicable to vehicles having arbitrary shapes, motions, and deformations in subsonic flow only. The P1.1 code employs zeroth-order (constant-potential) panels along with the data base and data-handling utilities of the SPAR finite-element structural-analysis program. These were incorporated because SOUSSA P1.1 originally was intended for the calculation of steady-state structural loads and unsteady aerodynamics for flutter and gust-response calculation in multidisciplinary structural-optimization computations employing the SPAR structural analysis. The SPAR components, however, are unnecessary for stand-alone use. More efficient data handling methods for stand-alone operation are available.

Subsequent to the completion of SOUSSA P1.1 several significant improvements have been incorporated, and others have been defined (ref. 5). Among the latter are implementation of higher-order panels, elimination of the SPAR components, transposition and revision of the solution algorithm to substantially reduce input/output operations, and improved implementation of the trailing-edge (Kutta) flow condition.

Some program improvements already incorporated in the SOUSSA code include the development of an "out-of-core" solver to permit the use of paneling schemes that lead to coefficient matrices too large to fit in the memory of modest-size computers; the replacement of the paneled wake by an analytical wake (reducing the cost of a typical run by about one-half) but retaining an option to use paneled wakes if needed (e.g., when there is another lifting surface in the wake); and replacing the rectangular integration of pressures by a Gaussian quadrature scheme to improve the accuracy of the calculated generalized aerodynamic forces. These improvements are incorporated in a replacement for the SOUSSA code (called UTSA) which is under development at a low level of effort.

Figure 3 (reproduced from ref. 5) compares a chordwise distribution of pressure coefficient C_p calculated by the SOUSSA surface-panel method with pressures measured on a clipped delta wing oscillating in pitch (ref. 20). The wing had a six-percent-thick circular-arc airfoil. The agreement is good and is representative of results obtained with this code. Figure 4 compares calculated and measured steady upper-surface pressures at two chordwise locations x on an outboard station (y=0.85) on the same clipped delta wing. Two points are to be made: First, in the range of angle of attack α (-2 deg to +2 deg) where pressure varies linearly, the agreement is excellent. Second, for this sharp-edge wing, the influence of the leading-edge vortex is substantial and begins at a low angle of attack. The latter behavior emphasizes the importance of our treatment of vortex-type flow separation to be discussed below. A phenomenological description of the relation between the vortex development and the pressure variation shown is given in ref. 21 (from which figure 4 was taken) and in Appendix A of ref. 20.

In addition to the subsonic capability of the SOUSSA program, a supersonic proof-of-concept surface-panel code has been written to implement linear-theory

algorithms developed in refs. 6 and 7. The code employs first-order panels and, like SOUSSA, is applicable to vehicles having arbitrary shapes, motions, and deformations. Validation and application of the code have begun.

The only significant difference between subsonic and supersonic formulations is in the expressions for the influence integrals B,C,D, F,G in equations (5) and (6) (see, e.g., ref.2). Other portions of the computations, such as paneling geometry and solution alorithms are common to both. Consequently, it is possible that the computational capability for supersonic flow derived from this proof-of-concept code will subsequently be incorporated into the subsonic code UTSA.

The status and near-term plans for linear-theory surface-panel methods, which are applicable to vehicles having arbitrary shapes, motions, and deformations, may be summarized as follows: As planned the SOUSSA program will be superseded by an improved program UTSA which incorporates first-order panels as well as other improvements indicated by earier work with SOUSSA. Ultimately, the code may include both subsonic and supersonic capabilities. Frequency-domain computations are most efficient for implementing linear theory, but a time-domain version is also retained for evaluation of the surface integral in the nonlinear methods described next. Specific activities include configuring the UTSA code for efficient use in interdisciplinary design processes, incorporating special elements to improve accuracy and efficiency near normalwash discontinuities (e.g., at control surfaces), completing the initial demonstration of the efficient computation of sensitivities of aerodynamic pressures and loads to variations in planform, and general check out and validation.

Nonlinear Theory

When the flow approaches transonic conditions and/or flow perturbations (e.g., angle of attack) become large, the nonlinear terms represented by F in equation (2) are no longer negligible, and the volume integral must be evaluated in combination with the surface-panel evaluation of the linear terms (refs. 9 to 11). For nonlinear problems it is important to note (1) that the Green's function depends on freestream Mach number, not local Mach number, and (2) that the integrand of the volume integral diminishes rapidly in magnitude with increasing distance from the body and its wake.

For application to nonlinear problems the integral-equation method has several features which make it particularly attractive for general, efficient computational implementation: (1) Evaluation of an integral is required rather than the numerical solution of a partial differential equation, which is a more sensitive process. (2) The volume integral need be treated only in the limited region of flow in which nonlinear terms are of significant magnitude rather than over an entire computational domain. In fact, as the integration proceeds away from the body, it is terminated when the integrand falls below a preselected threshhold value. (3) Required accuracy can be attained with relatively few computational grid points in the fluid (computational domain of the volume integral). (4) The code is numerically stable even when moderate-to-large time steps are employed. (5) Correct far-field boundary conditions are automatically imposed. This condition is particularly important for unsteady flow. Linear-theory behavior in the far field is inherent in the integral-equation solution. (6) When viscous flows are treated by the scalar/vector-potential decomposition (to be discussed below), interfacing (patching and matching) of regional solutions (e.g., inner viscous solution and outer inviscid solution) is not required. (7) Even for solution of the full-potential equation, there is no requirement for generating, imbedding, or interpolating surface-fitted computational grids.

In this section small-perturbation transonic attached flow will be considered first followed by large-perturbation subsonic and transonic flow conditions involving vortex-type flow separation in the form of thin wakes emanating from lifting-surface edges and finally flow conditions involving significant viscous effects which require solution of Navier-Stokes equations for attached or separated flow for which the scalar/vector-potential method is employed.

Small-Perturbation Transonic Flow: For proof-of-concept demonstration of transonic capability, only the small-perturbation terms were retained in the volume integral of equation (2), and the resulting time-domain computer code (ref. 11) was called SUSAN (Steady and Unsteady Subsonic Aerodynamics-Nonlinear). Figure 5 shows chordwise pressure distribution near the root of a rectangular wing as calculated by the SUSAN code and by a transonic small-perturbation finite-difference code. The shock is captured, and the agreement is quite good even though only a few elements were used to evaluate the volume integral, and the domain of integration extended only one chord length from the wing perimeter. Good agreement with measured pressures (from ref. 22) is shown in figure 6 for a sharp-edge wing under conditions involving supercritical flow over much of the chord.

Evolution of the lifting pressure ΔC_p on a wing oscillating slowly in pitch about the leading edge is shown in figure 7 at three times during a cycle of motion. Although only ten computational elements along the wing chord were used to evaluate the volume integral of the nonlinear terms, the build-up of lift and the appearance of a shockwave are clearly indicated. In this particular figure, the symbols shown are used only to distinguish the curves and do not indicate computational points.

The formulation described here and its implementation in the SUSAN code demonstrated the merits of the integral-equation method for transonic flow. However, no further development of the small-perturbation approximation is planned.

Subsonic/Transonic Flow with Vortex Separation: All of the preceding involved calculation of the velocity potential. For solving nonlinear problems, however, there are advantages in calculating velocities directly, especially when large velocity variations occur, when shocks are present, when thin-wake (vortex-like) flow separation from wing leading or side edges occurs (fig. 8), or even when trailing-edge wake deformations are significant. Taking the gradient of the integral equation for the potential (equation (2)) or alternatively applying the Green's-function method to the full-potential equation in the form (for steady state)

$$\nabla^2 \phi = \frac{-1}{\rho} \nabla \rho \cdot \nabla \phi \equiv Q \tag{7}$$

gives (ref. 8)

$$\bar{V}(x,y,z) = \bar{E}_\infty + \frac{1}{4\pi} \iint_{BODY} \frac{\bar{\omega} \times R}{R^3}\ dS + \frac{1}{4\pi} \iint_{WAKE} \frac{\bar{\omega} \times R}{R^3}\ dS \tag{8}$$

$$+ \frac{1}{4\pi} \iiint_{VOL.} \frac{Q}{R^2}\ \bar{E}_R dV$$

where ρ is the fluid density, $\bar{\omega}$ is the vorticity vector, R is the vector from "sending" point to "receiving" point, $\bar{E}_R$ is a unit vector in the R direction, and $\bar{E}_\infty$ is a unit vector in freestream direction.

Equation (8) is an expression for the velocity field $\bar{V}$ as the sum of four components: (1) freestream, (2) a surface integral which gives the velocity induced by the flow singularities representing the solid body, (3) a surface integral which gives the velocity induced by the vorticity representing the thin wake, and (4) a volume integral representing the compressibility terms (right-hand side of equation (7)). The integrand of this volume integral decreases more rapidly than the square of the distance from the body or vortex surface, so the domain of integration can be relatively small. The integrands in the three integrals are not independent, and solution is by iteration to satisfy the boundary conditions on the body and to deform the free vortex sheets into a force-free shape (ref. 8). Note that the form of the integrand shown in the body integral indicates the use of a vorticity distribution to represent a thin wing in some proof-of-concept calculations. One of the major generalizations of this method, to be initiated, consists of replacing this body integral with the UTSA surface-panel formulation so that transonic flow over bodies of arbitary shape, including vortex-type separation, can be calculated. Other planned improvements include (1) replacing the vortex-lattice model used in the wake integral for proof-of-concept calculations with the hybrid-vortex formulation (refs. 23 and 24) in which second-order distributed-vorticity panels are used to compute near-field influence, reducing to zeroth-order (discrete-vorticity) elements for far-field influence, (2) shifting the linear compressibility term $M^2 \phi_{xx}$ from volume integral to surface integral by solving

$$\nabla^2 \phi - M^2 \phi_{xx} = Q - M^2 \phi_{xx} \equiv Q_{nonlin} \tag{9}$$

instead of equation (7), thereby significantly reducing the region over which the volume integral needs to be evaluated, (3) replacing constant source strength with linearly varying source strength in the volume elements and introduing a threshold cutoff value for the integrand of the volume integral to terminate integration when the integrand diminishes to negligible magnitude. (4) accelerating convergence of the solution by possible use of shock fitting (ref. 8), (5) accounting for entropy changes across shockwaves (see, e.g., ref. 12). Code development for unsteady flow is in progress. Research on suitable configuration of these codes for efficient use in computer-aided interdisciplinary design will be a continuing activity.

Completion of the improvements listed above should provide a powerful tool for calculating transonic and/or free-vortex flows around arbitrary aircraft configurations with sharp leading edges or with specified separation line locations. Establishing the separation line on a vibrating wing, however, is a tough viscous-flow problem, but may be amenable to treatment by the scalar-vector potential method to be discusssed below. The importance of expediting this activity should be underscored. The ability to calculate accurately the complicated transonic vortical flows around highly swept wings and complete aircraft at high angles of attack is a key problem for the future development of highly maneuverable fighter aircraft and is already needed to improve the assessment and understanding of steady and transient flight loads and flutter problems of current combat aircraft. It should be especially noted that vortex-type flow separations produce typically detrimental effects on structural loads and flutter.

Figure 9 shows the calculated velocity field and shape of the free-vortex surface in a crossflow plane slightly downstream of the trailing edge of a delta wing with vortex sheets representing thin wakes emanating from leading and trailing edges as in figure 8. The volume integral (equation (8)) has not been included for this incompressible-flow calculation. The results compare quite favorably with the low-Mach-number

5

experiments of Hummel (ref. 25) even though relatively few vortex elements were used in this exploratory calculation. The leading-edge vortex core is clearly defined as is the incipient deformation of the trailing-edge vortex sheet into a trailing-edge core with rotation opposite to that of the leading-edge core. The corresponding spanwise distributions of lifting pressure ΔC_p are shown in figure 10 for crossflow planes at 0.7 and 0.9 of the root chord aft of the wing apex. Agreement with measured values is very good.

Inclusion of the volume integral (equation (8)) permits calculation of transonic flow. Figure 11 shows the spanwise distribution of upper-surface pressure C_{pu} and the flow field, including a captured shock, in a crossflow plane at 0.8 of the root chord aft of the apex of a delta wing (ref. 8). In this exploratory calculation the vortex sheet was not allowed to roll up enough to exert its full inductive effect on the wing surface before the vorticity was transferred into the vortex core. If an additional quarter turn of rollup were allowed, the pressure peak would be slightly higher and a little farther outboard, resulting in even better agreement with experiment. In contrast, the pressure peak from the Euler solution is considerably weaker and farther outboard than the experimental peak because of spatial and numerical diffusion in the Euler calculation.

Structural design loads do not occur at small-perturbation conditions but at limit load-factor conditions such as high angle of attack. Aeroelastic deformations are important. Wind-tunnel results may be of questionable accuracy because of large wall effects. The important influence of large perturbation conditions and free-vortex flows on structural design loads is typically detrimental, as is illustrated by the calculations shown in figure 12 (from ref. 26). Even if the linear and nonlinear spanwise load distributions shown were compared on the basis of same total normal force (same area under the curves), it is evident that the effect of the wing-tip vortex is to shift the load outboard and hence increase wing bending movements.

Linearized aerodynamic theory indicates that there should be no effect of angle of attack on flutter dynamic pressure. However, a detrimental effect typically does occur with increasing angle of attack (see, e.g., refs. 27 and 28). If adequate flutter margins are to be maintained when angle of attack is not near zero, the degradation must be predictable. Wind-tunnel testing of stiffness-scaled flutter models is not the answer because they are typically too weak to sustain more than very small static loads. Figure 13 shows experimental variation of flutter dynamic pressure with angle of attack for a stiff wing that was spring supported (ref. 29). The initial decline in flutter dynamic pressure between 0 and 7 deg is attributed to the effect of the tip vortex. Confirming calculations by methods just described are in early stages. The drastic decline beyond 7 deg is probably caused by flow separation progressing forward from the trailing edge. Prediction of that behavior will require solutions of Navier-Stokes equations as discussed below.

Summarizing the status of integral-equation methods for vortex-type (thin wake) flow separation: The hybrid-vortex method for low-Mach-number steady flow (refs. 23 and 24) is complete. Computations based on equation (8) for steady transonic flow with vortex-type separation and shockwaves have been demonstrated (ref. 8), and the corresponding unsteady code development is in progress. Major generalizations and improvements in efficiency are underway. Further developments for transonic flow, with or without vortex-type flow separation, will be based on equation (8).

Scalar/Vector-Potential Method: When viscous influences (other than thin wakes from lifting-surface edges) are important -- for example, boundary-layer effects on control-surface forces, shock/boundary-layer interaction, or flow separation from surfaces (fig. 1) -- solution of Navier-Stokes equations in some form is required. The approach taken here is a scalar/vector-potential (SVP) decomposition of the velocity field by use of the classical Helmholtz representation of a vector field as the sum of an irrotational part and a solenoidal part (refs. 13 to 15). Thus

$$\bar{v} = \text{grad } \phi + \text{curl } \bar{A} \tag{10}$$

where ϕ is again the scalar potential which is evaluated by the methods already described herein, and the vector potential $\bar{A}$ is related to the vorticity $\bar{\omega}$ by

$$\nabla^2 \bar{A} = -\bar{\omega} = -\text{curl } \bar{v} \tag{11}$$

The vorticity, in turn, is governed by the vorticity-dynamics equation

$$\frac{D}{Dt}\left(\frac{\bar{\omega}}{\rho}\right) - \frac{\bar{\omega}}{\rho} \cdot \text{grad } \bar{v} = \frac{1}{\rho} \text{curl } \bar{A}$$

$$= \frac{1}{\rho} \text{grad } T \times \text{grad } S + \frac{1}{\rho} \text{curl } \frac{1}{\rho} \text{div } (T + p\bar{I}) \tag{12}$$

6

which is obtained by taking the curl of Navier-Stokes equation for general, three-dimensional, unsteady, compressible, viscous, heat-conducting flow (ref. 13) to which the present formulation is fully equivalent. In equation (12), T is temperature, S is entropy, and $\bar{T}$ is stress tensor.

The formulation in equations (10) to (12) appears to be a computationally attractive alternative to direct solution of the Navier-Stokes equations in primitive variables. Methods of this type have been used for a long time for viscous incompressible flow, but they have not proved to be readily generalizable to compressible flow. The present formulation is quite general and is directly applicable to compressible flow. Since the outer region of the flow about an aircraft is essentially irrotational, an integral-equation implementation appears to be an especially attractive method of solution. The initial proof-of-concept code for two-dimensional incompressible flow has been used to calculate boundary layers on a flat plate (fig. 14), flow over an airfoil, and separated flow around a rectangle (fig. 15) -- all with good results (refs. 14 and 15). In particular, the calculation of flow around a rectangle (fig. 15) demonstrates the ability to calculate flows involving large regions of separation. The resulting velocity field shown in the figure illustrates that flow separation is predicted very satisfactorily even though separation was not imposed by any artificial means within the algorithm. These results are in excellent agreement with the finite-difference results of ref. 31. Application to a circulation-control airfoil is being initiated. For applications to turbulent flows this method, of course, requires a good turbulence model just as any other method does. In addition to its computational use, the SVP formulation has also generated considerable insight into the relations between surface boundary conditions, viscosity, vorticity and its diffusion (refs. 14 and 15).

Current activities are extending the proof-of-concept code to three dimensions and to compressible flow. The types of applications planned include viscous flow over lifting surfaces with and without control-surface deflection, lifting surfaces with flow separation from edges in compressible flow, and lifting surfaces with separated flow following a step change in angle of attack.

Summary of Integral-Equation Activities

The activities described here and the computational capabilities summarized in table I indicate that completion of this work will provide efficient and underlined unified treatment of flow over vehicles having arbitrary shapes, motions, and deformations at subsonic, transonic, and supersonic speeds up to high angles of attack. Moreover, the computational forms of the equations and the computational capabilities that are emerging appear to be well suited for repetitive use in design applications as well as for stand-alone use. As pointed out previously, the UTSA surface-panel program for attached flow may contain both subsonic and supersonic modules in a single program. Flow complexities, such as transonic nonlinearities, thin wakes, or viscous influences, are addressed only if and where they occur. Thus, if the volume-integral module is included with UTSA, the program implements the full-potential equation for transonic nonlinear attached flow. With modification for shock-generated entropy change, the program can apply also to flows with shocks of finite strength, including supersonic Mach numbers above the linear range, as long as shock-generated vorticity is of minor importance. If the hybrid-vortex module representing the free vortex sheets is also included, the code treats transonic flow with vortex-type separation. Finally, combination of the vector potential with these scalar-potential methods (SVP formulation) permits the formal equivalent of Navier-Stokes solutions for high angles of attack where flow separation from surfaces may occur (for example, on advanced fighter aircraft in combat maneuvers and in highly transient conditions) and also even for low angles of attack when control-surface deflections or deflection rates are large enough or shock waves are strong enough to cause significant boundary-layer thickening or separation. The latter conditions are particularly important for generating control forces and for design of active control systems.

FINITE-DIFFERENCE METHODS

The goal of this activity is to develop finite difference methods that can be used for aeroelastic analysis of complete aircraft. At the Langley Research Center, efforts based on transonic small perturbation (TSP) potential theory, full potential theory, and the Euler/Navier-Stokes equations are underway.

Transonic Small-Perturbation Equation

At the TSP level, development has progressed on two fronts--(1) extending the capability of the XTRAN3S code (ref. 32) through extensive modification and (2) developing a new program (ref. 33). Fig. 16 shows a sample wing/fuselage calculation made possible by modifying XTRAN3S (ref. 34). The wing has an RAE 101 airfoil section, 37 deg leading edge sweep angle, aspect ratio (AR) of 6, and taper ratio of one-third. The fuselage is a sting-mounted, axisymmetric body of revolution with fineness ratio (length/maximum diameter) of 7.66. Calculations were made for a flexible wing at free stream Mach number (M) of 0.91 and mean angle of attack (α) of 1 deg. Fig. 16 (a) shows the wing tip deflection as a function of time, and fig. 16 (b) shows the gridding used to represent the wing/fuselage. Figs. 16 (c) and 16 (d) show the instantaneous Mach number contours at the maximum and minimum tip deflections, respectively. The wing motion is the first bending mode at a reduced frequency (k) of 0.25. The contours

7

near the leading and trailing edges indicate local Mach numbers less than 0.85, and over the wing chord and fuselage, the contours indicate Mach numbers greater than 0.95.

A new TSP code, CAP-TSD (Computational Aeroelasticity Program-Transonic Small Disturbance) (ref. 33) has been developed at Langley. It solves the three-dimensional (3-D) TSP equation using an approximate factorization (AF) algorithm. The code is significantly more efficient than methods that use an alternating-direction-implicit (ADI) solution algorithm and can be used for aeroelastic analysis of complete aircraft. Fig. 17 shows comparisons of CAP-TSD (AF) and XTRAN3S (ADI) calculations with experimental data for a rigid F-5 wing pitching about zero mean angle at k = 0.137 (ref. 35). Pressures are shown at the 51 percent span station ($\bar{\eta}$). Upper surface pressures are shown in fig. 17 (a), and lower surface pressures are shown in fig. 17 (b). Both sets of calculations show good agreement with the measured data and are nearly identical to each other. The primary difference is that the AF solution requires only ten percent of the computer resources used in the ADI calculation. CAP-TSD has been used to compute steady flow past a wing/fuselage/tail model that was tested at DFVLR. In the test, M = 0.2, α = 0.15 deg. The wing is rectangular with RAE 101 airfoil sections (9 percent thickness ratio) and a full-span aspect ratio of 6. The horizontal tail is rectangular with RAE 101 airfoil sections (12 percent thicknessratio) and full-span aspect ratio of 3. The fuselage is an axisymmetric body of revolution with fineness ratio of 9.75. The mathematical representation of the model is shown in fig. 18 (a). Comparisons of computed and measured pressures on the wing and tail are shown in fig. 18 (b). Fig. 18 (c) shows comparisons of computed and measured pressures on the fuselage. In all cases, the computations and experiments are in good agreement.

Potential flow theory has been shown to give highly erroneous and even multivalued results when shock waves are in the flow field (refs. 36, 37). This is because shock-generated entropy is not modeled in potential flow formulations. A method for modeling nonisentropic effects in 2-D TSP theory was developed by Fuglsang and Williams (ref. 12) and extended to three dimensions by Gibbons et al. (ref. 38). The nonisentropic formulation was implemented by modifying the streamwise flux in the TSP equation to account for entropy jumps across shock waves. This alleviates the phenomena of multiple solutions and highly inaccurate loading predicted by isentropic potential methods. Fig. 19 shows an example of calculated lift as a function of angle of attack for isentropic and nonisentropic formulations. An Euler calculation is included at one deg angle of attack. Without the nonisentropic corrections, the calculated lift is too large. When the corrections are included, the calculated lift is less and agrees with the Euler calculation at the point where such data is available.

Full-Potential Equation

A method for modeling shock-generated entropy in the unsteady full-potential (FP) formulation has been developed at Langley (ref. 39). The method is an extension of the steady-flow method of Hafez and Lovell (ref. 40). Fig. 20 shows the instantaneous pressures on an NACA 0012 airfoil oscillating in pitch about its quarter chord. In this case, M = 0.755, $\alpha(t)$ = (0.016 + 2.51sin(kt)) deg, and k (based on semichord) = 0.0814. Fig. 20 (a) shows a comparison of the isentropic full-potential method, a TSP method (denoted by "TSD" on the figure) (ref. 41), and experimental data (ref. 42). Fig. 20 (b) shows isentropic and nonisentropic full potential methods, along with the measured data. When entropy corrections are used, more accurate modeling of the shock is obtained, and agreement with the measured data is improved.

Currently, efforts are underway to extend the full potential method to three dimensions. The proposed method will have the capability to do aeroelastic analysis for flows in the subsonic, transonic, and supersonic speed ranges.

Euler/Navier-Stokes Equations

Research is being conducted to develop methods for obtaining time-accurate unsteady solutions of the Euler/Navier-Stokes equations. These methods are used to solve the Navier-Stokes equations, with solutions of the Euler equations obtained by turning off the viscous terms. The existing codes are used to march in time to steady state and currently are being modified to be made time-accurate. An effort is underway to correlate Navier-Stokes calculations with pressure data measured in the Langley Research Center 0.3-meter Transonic Cryogenic Tunnel. Unsteady transonic pressures were measured on a 14-percent-thick supercritical airfoil at cryogenic temperatures for M between 0.65 and 0.74 and at Reynolds numbers based on airfoil chord (Rc) between 6 million and 35 million (ref. 43). The model is shown in fig. 21 (a). The open symbols in fig. 21 (b) show test conditions where the effects of frequency on the unsteady pressures were examined, and the solid symbols show where the effects of frequency and amplitude were studied. Steady pressure distributions at Rc = 6 million (open symbols) and at Rc = 30 million (solid symbols) are shown in fig. 21 (c). The results of this study may be used to determine when various forms of the Navier-Stokes equations can be used (e. g., thin-layer or the full equations) and may be used to evaluate methods that couple viscous flow models with inviscid methods.

An implicit upwind code that can be used to calculate massively separated 2-D flows (ref. 44) is available for use in the correlation study. It uses van Leer flux-vector splitting and is first-order accurate in time and second-order accurate in space. The

8

method can be used for time marching to steady-state solutions, but it is not time-accurate and cannot model unsteady flow. An example of the capability of this code is shown in fig. 22. Even though the code is not time accurate, the example shows the variation in loads that can occur when marching to steady state. It shows computation of laminar flow about a 12-percent-thick Joukowski airfoil at 53 deg angle of attack at minimum lift (fig. 22 (a)), increasing lift (fig. 22 (b)), and maximum lift (fig. 22 (d)) for a Strouhal number of 0.166. The time history of the lift is shown in fig. 22 (c). At minimum lift, a strong counterclockwise vortex has just been shed from the trailing edge. There is a weak region of clockwise vorticity one-half chord behind the airfoil and a strong region of clockwise vorticity, which persists throughout the entire cycle, at the leading edge. The flow near the upper surface is broken into several cells of vorticity. As the lift increases, the trailing edge vortex breaks away and weakens as the region of clockwise vorticity behind the airfoil increases in strength. The vorticity near the upper surface becomes predominantly counterclockwise. Current efforts are aimed at extending this capability to time-accurate analysis of 2D unsteady flows.

A steady-flow Navier-Stokes method (ref. 45) is available for analysis of 3-D wings. The convective and pressure terms are upwind differenced, using a flux-vector splitting method. The shear stress and heat transfer terms are centrally differenced. The resulting algorithm is second-order accurate in space. An implicit, spatially factored algorithm, which is fully vectorized for the Control Data Corporation VPS 32, is used to provide efficient solutions. Efforts also are underway to extend this capability to 3D time-accurate analysis. An example of calculations made using this method is shown in fig. 23. It shows the contours of the calculated total pressures on an AR = 1 delta wing (75 deg leading-edge sweep angle) at M = 0.3 and α = 20.5 deg. Solutions were obtained by marching in time to steady state. Primary and secondary vorticies are evident on the upper surface. Close examination of the surface velocities indicates a tertiary separation outboard of the secondary vortices. This type of flow field also was observed in a related experiment (ref. 25).

Fig. 24 shows contours of measured total pressures on the same delta wing at the same flow conditions used in the previously mentioned Navier-Stokes calculations. These steady-flow data were measured in the Basic Aerodynamic Research Tunnel at Langley (ref. 46) and show good agreement with the calculated data in fig. 23.

Summary of Finite-Difference Activities

Areas of current activity in the development of finite-difference methods are shown in fig. 25. Methods based on TSP theory are being applied to configurations as complex as complete aircraft. Unsteady full-potential methods are being developed for 3-D configurations with the goal being to use such methods for aeroelastic analysis of complete aircraft. Steady, time-marching Navier-Stokes methods are available for airfoil and for isolated wings. Those methods are currently being made time-accurate.

CONCLUDING REMARKS

Some problems, progress, and plans in the development of steady and unsteady computational aerodynamics for use in aeroelastic analysis and design have been reviewed. The primary focus has been on applications to (1) vehicles having arbitrary shapes, motions, and deformations, (2) appropriate design and operating conditions, especially for transonic speeds and high angles of attack, (3) efficient computation of aerodynamics and aeroelastic behavior for both design and analysis. Current and future activities have been highlighted.

REFERENCES

1. Morino, Luigi: A General Theory of Unsteady Compressible Potential Aerodynamics. NASA CR-2464, 1974.

2. Morino, Luigi; and Chen, Lee-Tzong: Indicial Compressible Potential Aerodynamics Around Comlex Aircraft Configurations. In "Aerodynamic Analyses Requiring Advanced Computers" NASA SP-347, Part II, pp. 1067-1110, 1975.

3. Morino, Luigi: Steady, Oscillatory, and Unsteady Subsonic and Supersonic Aerodynamics - Production Version (SOUSSA P1.1) - Vol. I, Theoretical Manual. NASA CR-159130, 1980.

4. Smolka, Scott A.; Preuss, Robert D.; Tseng, Kadin; and Morino, Luigi: Steady, Oscillatory, and Unsteady Subsonic and Supersonic Aerodynamics - Production Version 1.1 (SOUSSA P1.1), Vol. II - User/Programmer Manual. NASA CR 159131, 1980.

5. Yates, E. Carson, Jr.; Cunningham, Herbert J.; Desmarais, Robert N.; Silva, Walter A.; and Drobenko, Bohdan: Subsonic Aerodynamic and Flutter Characteristics of Several Wings Calculated by the SOUSSA P.1.1 Panel Method. AIAA Paper 82-0727, 1982.

6. Freedman, Marvin I.; Sipcic, Slobodan; and Tseng, Kadin: A First-Order Green's Function Approach to Supersonic Oscillatory Flow - A Mixed Analytic and Numerical Treatment. NASA CR-172207, 1984.

7. Freedman, Marvin I.; and Tseng, Kadin: A First-Order Time-Domain Green's Function Approach to Supersonic Unsteady Flow. NASA CR-172208, 1985.

8. Kandil, Osama A.; and Yates, E. Carson, Jr.: Computation of Transonic Vortex Flows Past Delta Wings - Integral Equation Approach. AIAA Journal, Vol. 24, No. 11, November 1986, pp. 1729-1736.

9. Morino, Luigi; and Tseng, Kadin: Time-Domain Green's Function Method for Three-Dimensional Nonlinear Subsonic Flows. AIAA Paper 78-1204, 1978.

10. Tseng, K. and Morino, L.: Nonlinear Green's Function Method for Unsteady Transonic Flows. In "Transonic Aerodynamics", edited by David Nixon. AIAA Series, Progress in Aeronautics and Astronautics, Vol. 81, 1982, pp. 565-603.

11. Tseng, K.: Nonlinear Green's Function Method for Transonic Potential Flow. Ph.D. Dissertation, Boston University, 1983.

12. Fuglsang, Dennis F.; and Williams, Marc H.: Non-Isentropic Unsteady Transonic Small Disturbance Theory. AIAA Paper 85-0600, 1985.

13. Morino, Luigi: Scalar/Vector Potential Formulation for Compressible Viscous Unsteady Flows. NASA CR-3921, 1985.

14. Morino, L.: Helmholtz Decomposition Revisited: Vorticity Generation and Trailing Edge Condition. Part 1: Incompressible Flows. Computational Mechanics, Vol. 1, 1986, pp. 65-90.

15. Morino, L.; Bharadvaj, B. K.; and Del Marco, S. P.: Helmholtz Decomposition and Navier-Stokes Equations. In "Proceedings of International Conference on Computational Mechanics", May 25-29, 1986, Tokyo, Japan.

16. Soohoo, P.; Noll, R. B.; Morino, L.; and Hamm, N. D.: Rotor Wake Effects on Hub/Pylon Flow. Vol. I, Theoretical Formulation . Applied Technology Laboratory, U. S. Army Research and Technology Laboratories (AVRADCOM), Fort Eustis, VA, USARTL-TR-78-1A, 1978, p. 108.

17. Morino,L.; Kaprielian, Z., Jr.; and Sipcic, S. R.: Free Wake Analysis of Helicopter Rotors. Vertica, Vol. 9, No. 2, 1985, pp. 127-140.

18. Morino, L.; and Bharadvaj, B. K.: Two Methods for Viscous and Inviscid Free-Wake Analysis of Helicopter Rotors. CCAD-TR-85-04-R, Boston University, 1985.

19. Bharadvaj, B. K.; and Morino, L.: Free-Wake Analysis of Helicopter Rotors: A Boundary Element Approach. BETECH 86, Proceedings of the 2nd Boundary Element Technology Conference, MIT, USA, pp. 291-303, Computational Mechanics Publications, 1986.

20. Hess, Robert W.; Cazier, F. W.; and Wynne, Eleanor C.: Steady and Unsteady Transonic Pressure Measurements on a Clipped-Delta Wing for Pitching and Control-Surface Oscillations. NASA TP 2594, 1986.

21. Yates, E. Carson, Jr.; and Olsen, James J.: Aerodynamic Experiments with Oscillating Lifting Surfaces - Review and Preview. AIAA Paper 80-0450. Invited Lecture given at AIAA 11th Aerodynamic Testing Conference, Colorado Springs, March 1980.

22. Knechtel, Earl D.: Experimental Investigation at Transonic Speeds of Pressure Distributions over Wedge and Circular-Arc Airfoil Sections and Evaluation of Perforated Wall Interference. NASA TN D-15, 1959.

23. Kandil, O. A.; Chu, L. C.; and Yates, E. C., Jr.: Hybrid Vortex Method for Lifting Surfaces with Free Vortex Flow. AIAA Paper 80-0070, 1980.

24. Kandil, O. A.; Chu, L.; and Turead, T.: A Nonlinear Hybrid Vortex Method for Wings at Large Angle of Attack. AIAA Journal, Vol. 22, No. 3, March 1984.

25. Hummel, D. J.: On the Vortex Formation Over a Slender Wing at Large Angles of Incidence. AGARD CP 247, 1978.

26. Kandil, Osama A.: Prediction of the Steady Aerodynamic Loads on Lifting Surfaces Having Sharp-Edge Separation. Ph.D. dissertation, Virginia Polytechnic Institute and State University, 1974.

27. Houwink, R.; Kraan, A. N.; and Zwaan, R. J.: Wind-Tunnel Study of the Flutter Characteristics of a Supercritical Wing. Journal of Aircraft, Vol. 19, No. 5, May 1982, pp. 400-405.

28. Yates, E. Carson, Jr.; Wynne, Eleanor C.; and Farmer, Moses G.: Effects of Angle
     of Attack on Transonic Flutter of a Supercritical Wing. Journal of Aircraft,
     Vol. 20, No. 10, October 1983, pp. 841-847.

29. Farmer, Moses G.: A Two-Degree-of-Freedom Flutter Mount System with Low Damping
     for Testing Rigid Wings at Different Angles of Attack. NASA Technical Memorandum
     83302, 1982.

30. Howarth, L.: On the Solution of the Laminar Boundary Layer Equations.
     Proceedings of the Royal Society A, London, 1938, p. 164.

31. Fromm, J. E.: and Harlow, F. H.: Numerical Solution of the Problem of Vortex
     Street Development. Physics of Fluids, Vol. 6, No. 7, 1963.

32. Borland, C. J.; and Rizzetta, D. P.: Nonlinear Transonic Flutter Analysis. AIAA
     Journal, Vol. 20, No. 11, November 1982, pp. 1606 - 1615.

33. Batina, John T.; Seidel, David A.; Bland, Samuel R.; and Bennett, Robert M.:
     Unsteady Transonic Flow Calculations for Realistic Aircraft Configurations. AIAA
     Paper 87-0850, 1987.

34. Batina, J. T.: Unsteady Transonic Flow Calculations for Wing/Fuselage
     Configurations. AIAA Journal, Vol. 23, No. 12, December 1986, pp. 897 - 903.

35. Tijdeman, H.; Van Nunen, J. W. G.; Kraan, A. N.; Persoon, A. J.; Poestkoke, R.;
     Roos, R.; Schippers, P.; and Siebert, C. M.: Transonic Wind Tunnel Tests on an
     Oscillating Wing with External Stores. AFFDL-TR-78-194, 1978.

36. Steinhoff, John; and Jameson, Antony: Multiple Solutions of the Transonic
     Potential Flow Equation. AIAA Journal, Vol. 20, No.z11, November 1982, pp. 1521 -
     1525.

37. Salas, M. D.; and Gumbert, C. R.: Breakdown of the Conservative Potential
     Equation. AIAA Paper 83-0367, 1983.

38. Gibbons, M. D.; Whitlow, W., Jr.; and Williams, M. H.: Nonisentropic Unsteady
     Three Dimensional Small Disturbance Potential Theory. AIAA Paper 86-0863, 1986.

39. Whitlow, Woodrow, Jr.; Hafez, Mohamed M.; and Osher, Stanley J.: An Entropy
     Correction Method for Unsteady Full Potential Flows with Strong Shocks. AIAA
     Paper 86-1768-CP, 1986.

40. Hafez, M.; and Lovell, D.: Entropy and Vorticity Corrections for
     Transonic Flows. AIAA Paper 83-1926, 1983.

41. Whitlow, Woodrow, Jr.: XTRAN2L: A Program for Solving the
     General-Frequency Unsteady Transonic Small Disturbance Equation. NASA TM
     85723, 1983.

42. Landon, R. H.: NACA 0012. Oscillatory and Transient Pitching. Compendium of
     Unsteady Aerodynamic Measurements, AGARD Report No. 702, 1982.

43. Hess, Robert W.; Seidel, David A.; Igoe, William B.; and Lawing, Pierce L.:
     Highlights of Unsteady Pressure Tests on a 14 Percent Supercritical Airfoil at
     High Reynolds Number, Transonic Condition. AIAA Paper 87-0035, 1987.

44. Rumsey, C. L.: Time-Dependent Navier-Stokes Computations of Separated Flows Over
     Airfoils. AIAA Paper 85-1684, 1985.

45. Thomas, J. L.; Taylor, S. L.; and Anderson, W. K.: Navier-Stokes Computations of
     Vortical Flows over Low Aspect Ratio Wings. AIAA Paper 87-0207, 1987.

46. Kjelgaard, Scott O.; Sellers, William L. III; and Weston, Robert P.: The
     Flowfield Over A 75 Degree Swept Delta Wing At 20.5 Degrees Angle Of Attack. AIAA
     Paper 86-1775, 1986.

Table 1.-Summary of Integral-Equation Activities.

α Range \ M Range	Subsonic	Transonic	Supersonic
Low (attached flow) w/large control deflection	UTSA SVP	Nonlinear UTSA SVP	UTSA
Moderate (vortex separation) w/large control deflection	UTSA + Hybrid vortex SVP	Nonlinear UTSA + Hybrid vortex SVP ·	
Large (separated flow) w/ or w/o control deflection	SVP SVP	SVP SVP	


```
1980                                                      1990
 |___|___|___|___|___|___|___|___|___|___|

 ┌──────────────────────────────────────────┐
 │ Sub/supersonic integral eq. method for complete a/c │
 ├──────────────────────────────────────────┤
 │  Linear              Nonlinear            │
 └──────────────────────────────────────────┘
                          ↓
 ┌──────────────────────────────────────────┐
 │      2D and  3D Transonic methods         │
 ├──────────────────────────────────────────┤
 │  Small perturb.; Full potential; Euler eq.; │Navier-Stokes eq.│
 └──────────────────────────────────────────┘
                       ⤫
 ┌──────────────────────────────────────────┐
 │          Viscous flow effects             │
 ├──────────────────────────────────────────┤
 │  Edge separation; B. L. effect; shock/B. L.; │Surface sep.│
 └──────────────────────────────────────────┘
```

═══ Deleted from original plan   ☐ Added to original plan
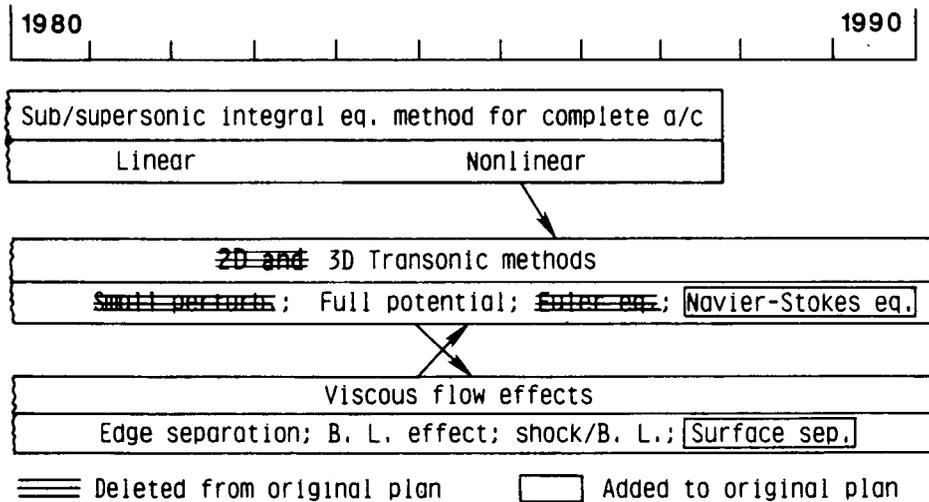
Goal: Validated computational methods for evaluating steady and
unsteady loads on aircraft having arbitrary shapes, motions, and
deformations (including control surfaces) in subsonic, transonic,
and supersonic flow up to high angles of attack

Justification: These methods are needed to evaluate and study
structural loads, aerodynamic coefficients, stability character-
istics, dynamic loads, and flutter in the analysis and design of
advanced high-performance aircraft, including fighters capable
of supermanuverability

Fig. 1 - Integral-equation program in unsteady aerodynamics

12
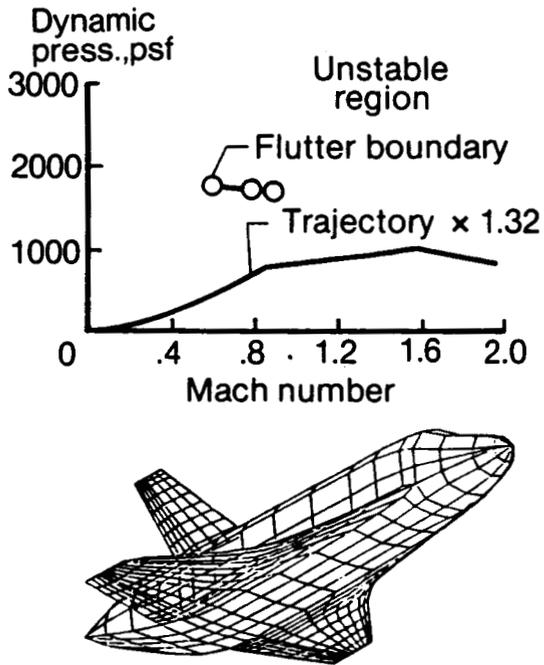
Fig. 2 - Shuttle orbiter flutter analysis by integral-equation method
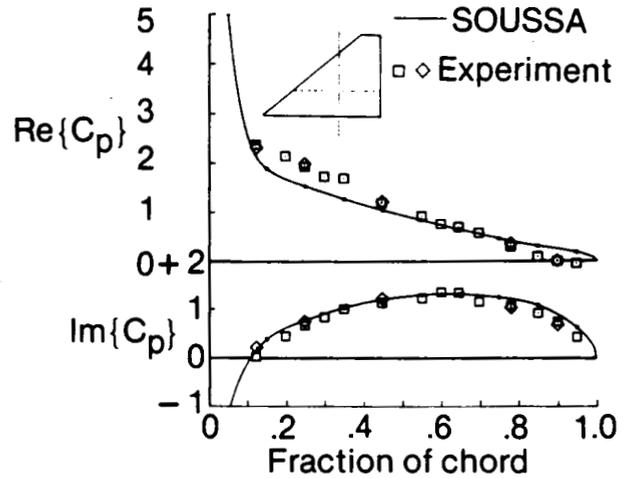
Fig. 3 - Unsteady surface pressures on clipped-delta wing at Mach number 0.4, reduced frequency 0.66
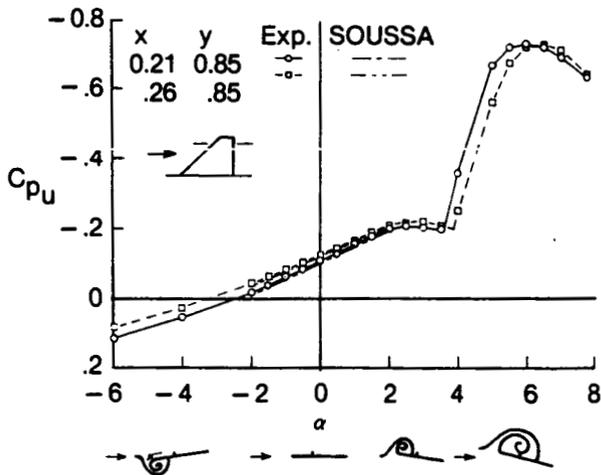
Fig. 4 - Effect of angle of attack on steady pressures for clipped-delta wing with 6-percent biconvex airfoil at Mach number 0.4, Reynolds number 2.x10⁶
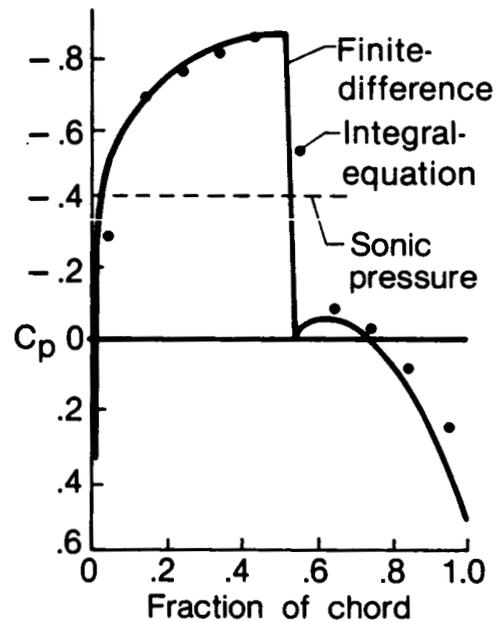
Fig. 5 - Steady pressures near root of aspect-ratio 6 rectangular wing with NACA 0012 airfoil at Mach number 0.82, α=0
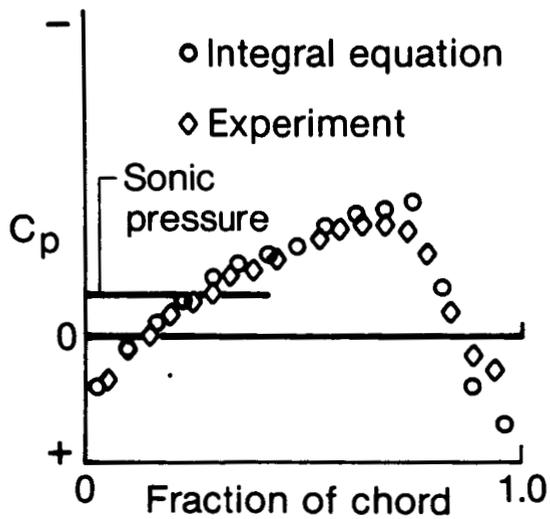
Fig. 6 - Steady pressures for aspect-
ratio 4 rectangular wing with 6% bi-
convex airfoil at Mach number 0.908,
$\alpha = 0$
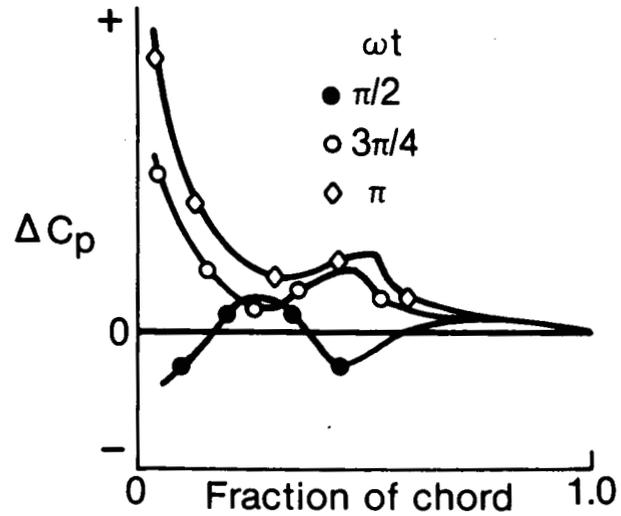
Fig. 7 - Unsteady pressures calculated
with SUSAN code for aspect-
ratio 5 rectangular wing with NACA
64A006 airfoil pitching at reduced
frequency 0.06, Mach number 0.875
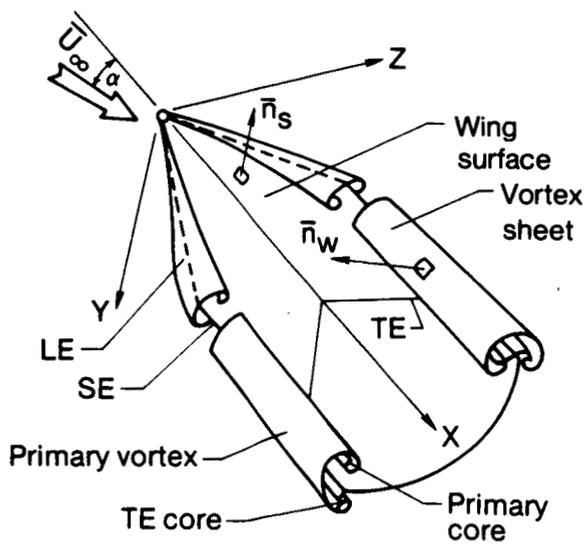
Fig. 8 - Sketch of vortex sheets separating
from wing edges

Experiment

Calculation
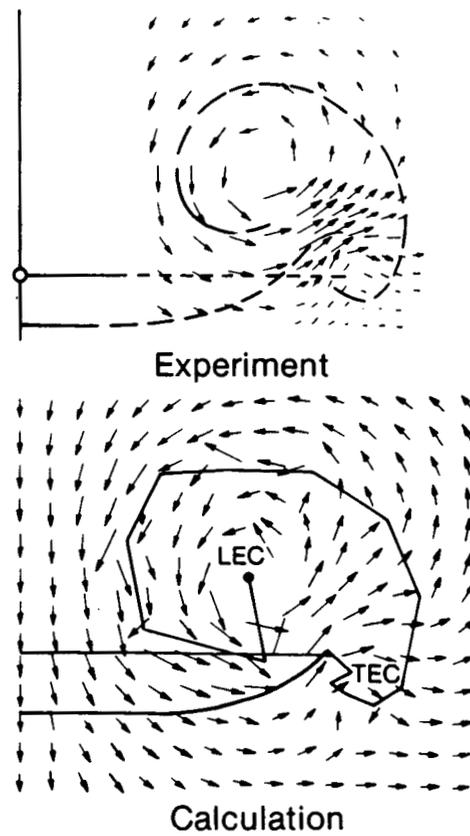
Fig. 9 - Flow field behind aspect-
ratio 1 delta wing at $\alpha = 20.5^\circ$

14
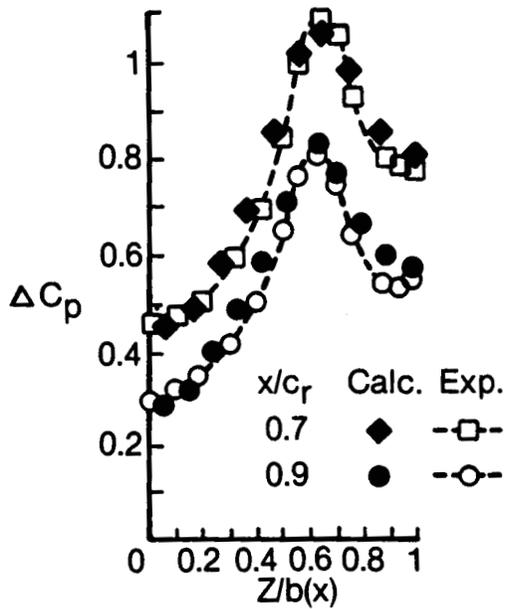
Fig. 10 - Steady pressures on aspect-
ratio 1 delta wing at $\alpha=20.5^\circ$
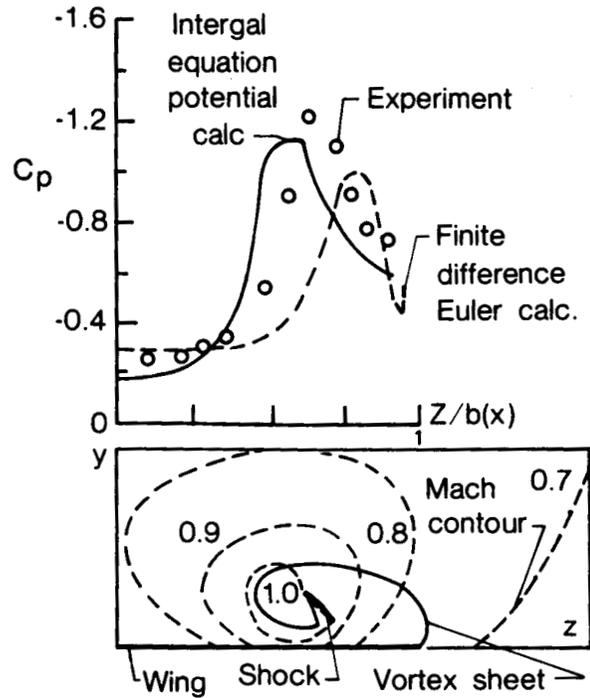
Fig. 11 - Steady pressures on aspect-
ratio 1.5 delta wing at Mach number 0.7,
$\alpha=15.^\circ$, $x/c_r=0.8$
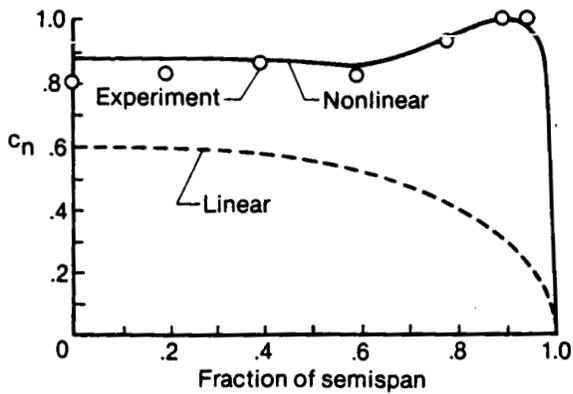
Fig. 12 - Steady spanwise variation of local
normal-force coefficient for aspect-
ratio 1 rectangular wing at $\alpha=19.4^\circ$
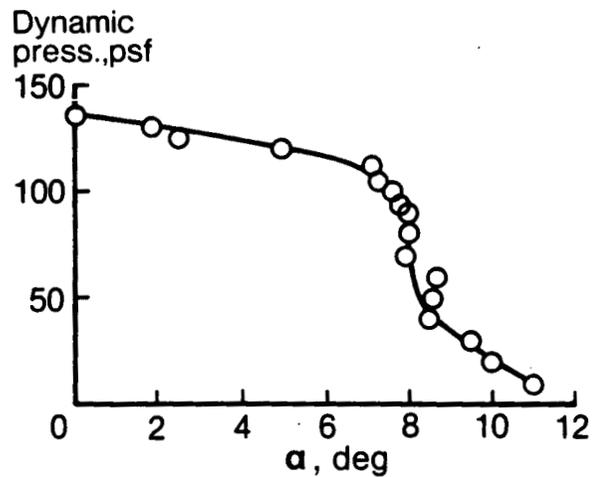
Fig. 13 - Effect of angle of attack on
flutter of aspect-ratio-6 rectangular
wing with NACA 64A010 airfoil

15

Distance from plate

0.6

Scalar/vector potential

Howarth (ref **30**)

0.0

Velocity, fraction of freestream

1.0
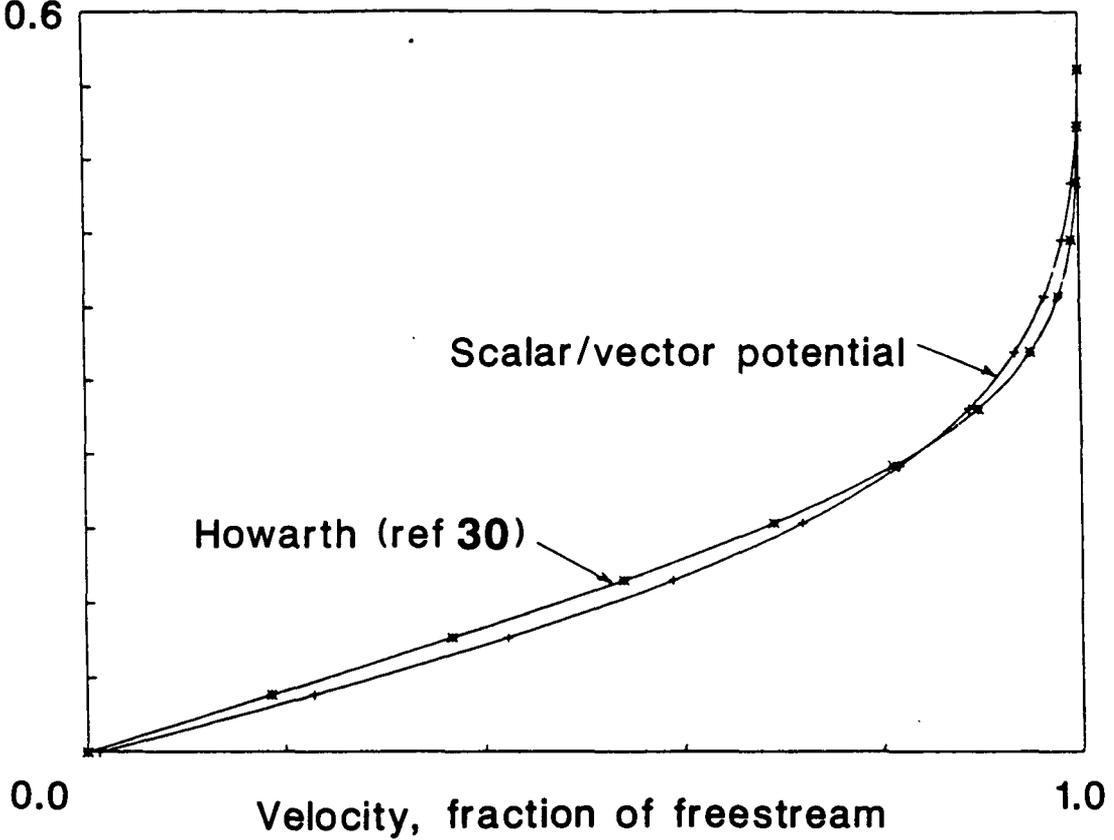
Fig. 14 - Velocity in laminar boundary layer on a flat plate in incompressible flow
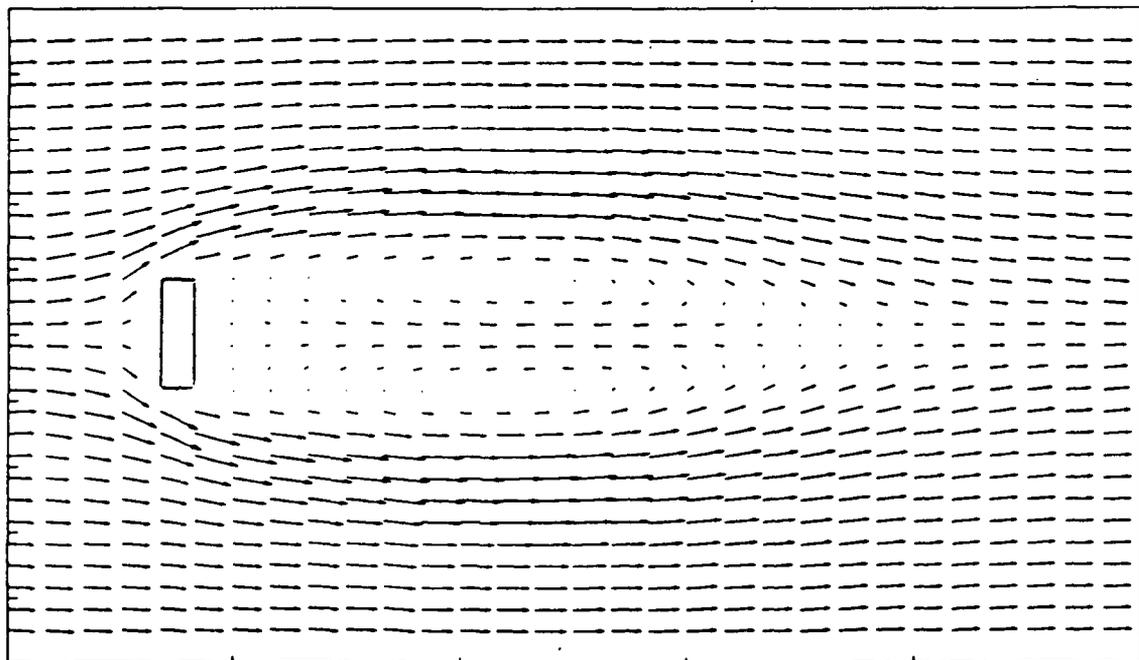
Fig. 15 - Velocity field around a rectangle in incompressible flow
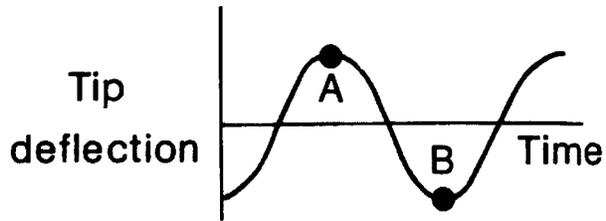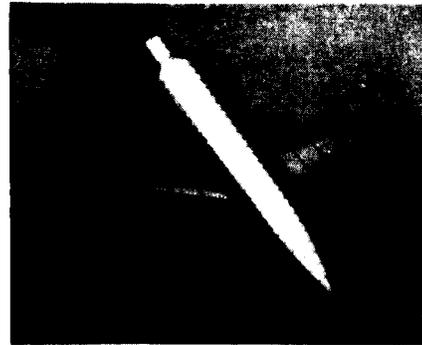
(a) Tip deflection

(b) Wing/fuselage gridding
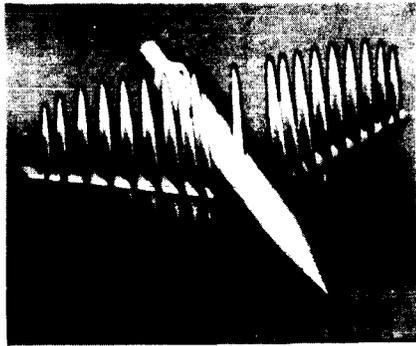
(c) Maximum tip deflection (A)
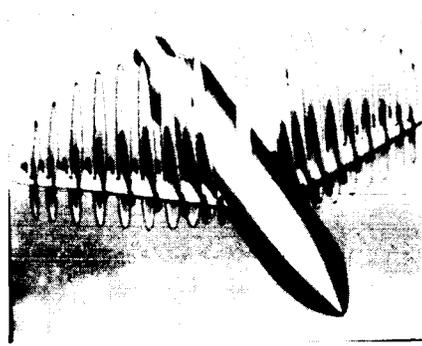
(d) Minimum tip deflection (B)

Fig. 16 - Unsteady transonic calculations for RAE wing/fuselage at Mach
number 0.91, α = 1 deg
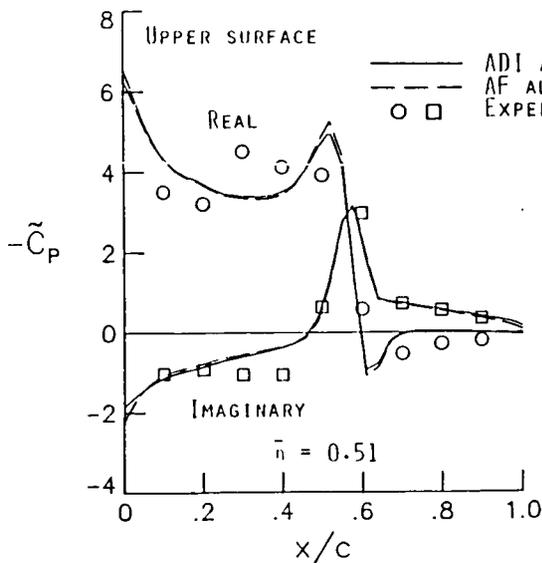
(a) Upper surface
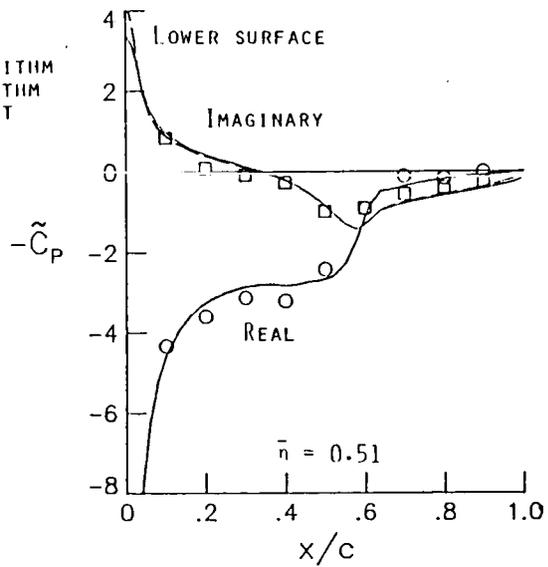
(b) Lower surface

Fig. 17 - First harmonic of unsteady pressures on F-5 wing at Mach number
0.9, α = 0 deg, k = 0.137

17
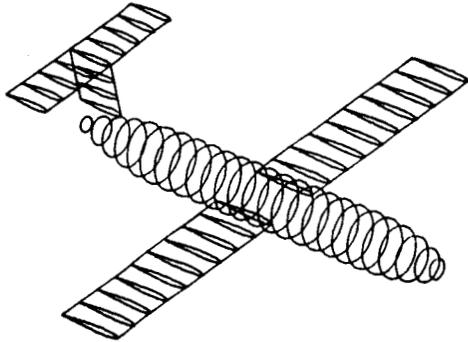
(a) Mathematical model
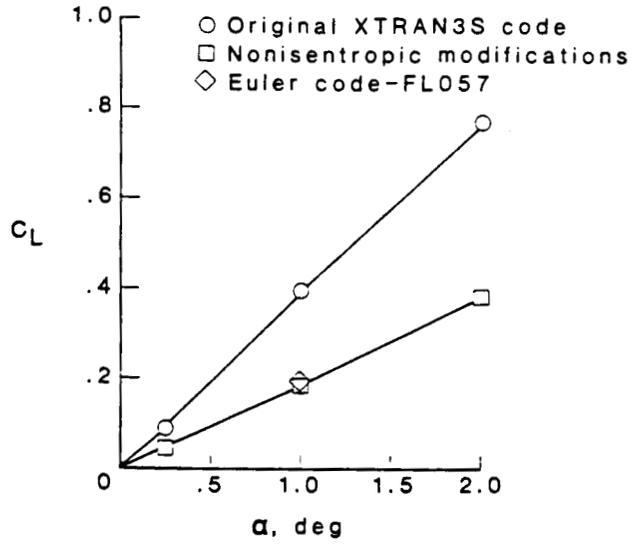
Fig. 19 - Calculated lift on a rectangular wing with NACA 0012 sections at Mach number 0.82
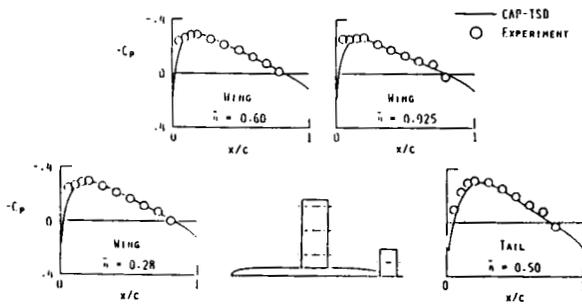
(b) Wing and tail pressures
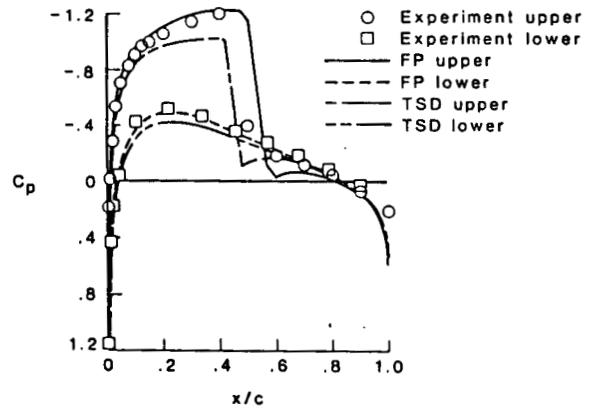
(a) Isentropic vs. experiment
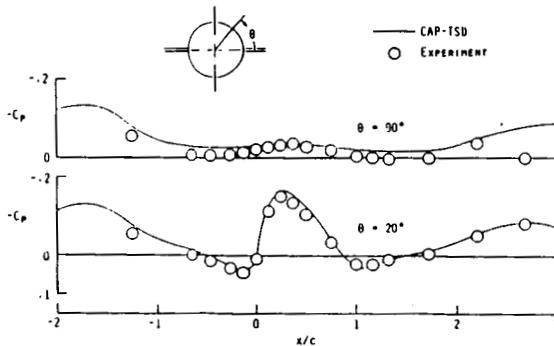

(c) Fuselage pressures

Fig. 18 - Steady flow computations for DFVLR model at Mach number 0.2, α = 0.15 deg
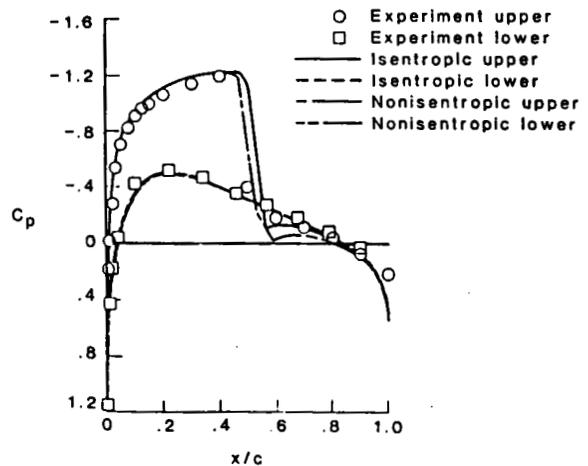
(b) Isentropic and nonisentropic vs. experiment

Fig. 20 - Unsteady pressures on an NACA 0012 airfoil at Mach number 0.755, α(t) = (0.016 + 2.51sin(kt)) deg, kt = 168 deg

18

(a) Model
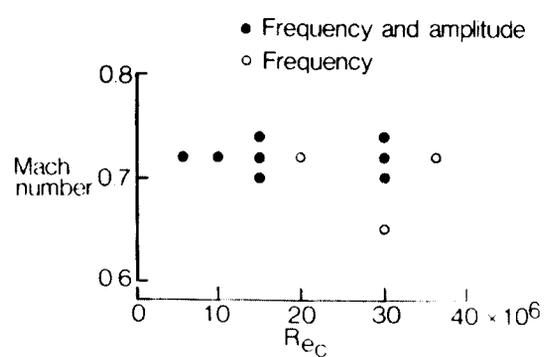
(b) Test conditions
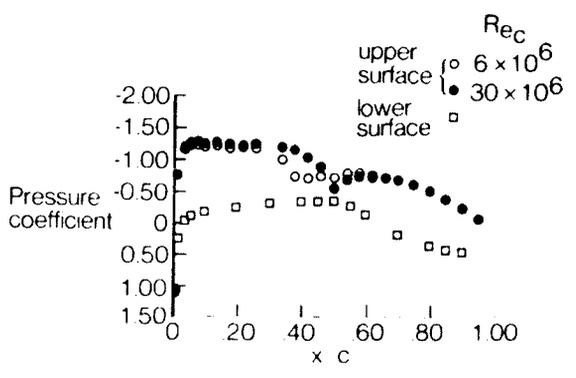
(c) Steady pressure distributions at Mach number 0.72, α = 1.5 deg

Fig. 21 - Study of Reynolds number effects on unsteady pressures

(a) Minimum lift

(b) Increasing lift
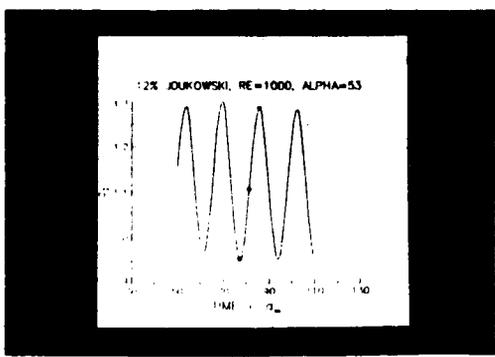
(c) Lift history
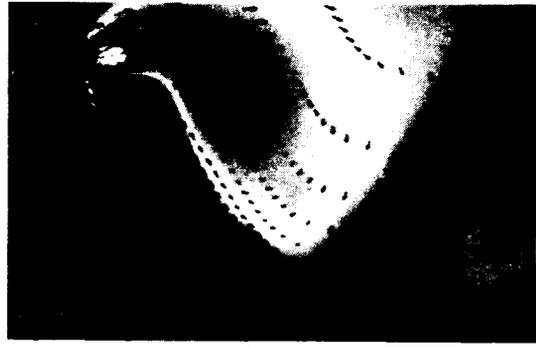
(d) Maximum lift

Fig. 22 - Computation of two-dimensional flow separation

19
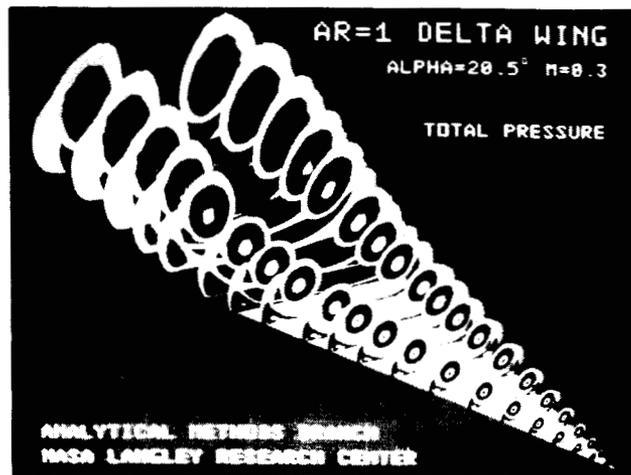
Fig. 23 - Calculated total pressure contours
on a 75 deg delta wing at Mach number
0.3, α = 20.5 deg, Reynolds number = 0.95
million
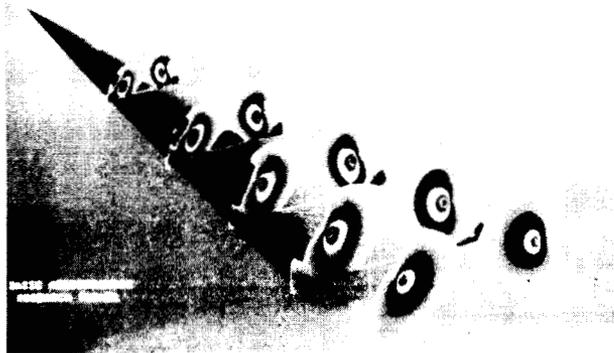
Fig. 24 - Measured total pressure contours
on a 75 deg delta wing at Mach number 0.3,
α = 20.5 deg, Reynolds number = 1 million

CONFIGURATION EQUATION LEVEL	AIRFOIL	WING	WING/BODY	COMPLETE AIRCRAFT
TRANSONIC SMALL PERTURBATION		X	X	X
FULL POTENTIAL		X	X	
EULER/ NAVIER-STOKES	X	X		

Fig. 25 - Summary of finite-difference activities

20

1. Report No. NASA TM-89133	2. Government Accession No.	3. Recipient's Catalog No.
4. Title and Subtitle Development of Computational Methods for Unsteady Aerodynamics at the NASA Langley Research Center		5. Report Date March 1987
		6. Performing Organization Code
7. Author(s) E. Carson Yates, Jr. Woodrow Whitlow, Jr.		8. Performing Organization Report No.
9. Performing Organization Name and Address NASA Langley Research Center Hampton, VA 23665-5225		10. Work Unit No. 505-63-21
		11. Contract or Grant No.
12. Sponsoring Agency Name and Address National Aeronautics and Space Administration Washington, DC 20546-0001		13. Type of Report and Period Covered Technical Memorandum
		14. Sponsoring Agency Code

15. Supplementary Notes Keynote paper presented in Workshop on Future Research on Transonic Unsteady Aerodynamics and Its Aeroelastic Applications at the 63rd meeting of the AGARD Structures and Materials Panel in Athens, Greece, 28 Sep - 3 Oct 1986.

16. Abstract

Progress in the development of computational methods for steady and unsteady aerodynamics has perennially paced advancements in aeroelastic analysis and design capabilities. These capabilities, in turn, are of growing importance in the analysis and design of high-performance aircraft as well as other types of flight vehicles. Consequently, considerable effort has been directed toward the development of appropriate unsteady-aerodynamic methodology in the NATO countries and elsewhere. This paper reviews the contributions to those efforts at the NASA Langley Research Center. Specifically, the current scope, recent progress, and plans for research and development of both integral-equation and finite-difference methods for inviscid and viscous flows are discussed, and example applications are shown. Although the great bulk of the effort in recent years has focused on finite-difference solution of the transonic small-perturbation equation, the integral-equation program is given primary emphasis here because it is less well known. Integral-equation methods for aircraft of arbitrary shape in inviscid or viscous flow, in all speed ranges, and at low-to-high angles of attack are addressed.

17. Key Words (Suggested by Author(s)) Unsteady Aerodynamics Transonic Aerodynamics Viscous Flow	18. Distribution Statement Unclassified - Unlimited Subject Category 02

19. Security Classif. (of this report) Unclassified	20. Security Classif. (of this page) Unclassified	21. No. of Pages 21	22. Price A02